IEEE Photonics Journal
An IEEE Photonics Society Publication

Open Access

A Novel Method Based on Digital Image Processing Technique and Finite Element Method for Rapidly Modeling Optical Properties of Actual Microstructured Optical Fibers

Volume 8, Number 6, December 2016

Jianshe Li, *Student Member, IEEE*
Shuguang Li
Guanghua Gu
Hui Li
Qiang Liu
Zhenkai Fan
Hailiang Chen, *Student Member, IEEE*
Xiaoming Han
Yuanyuan Zhao
Pu Zhang

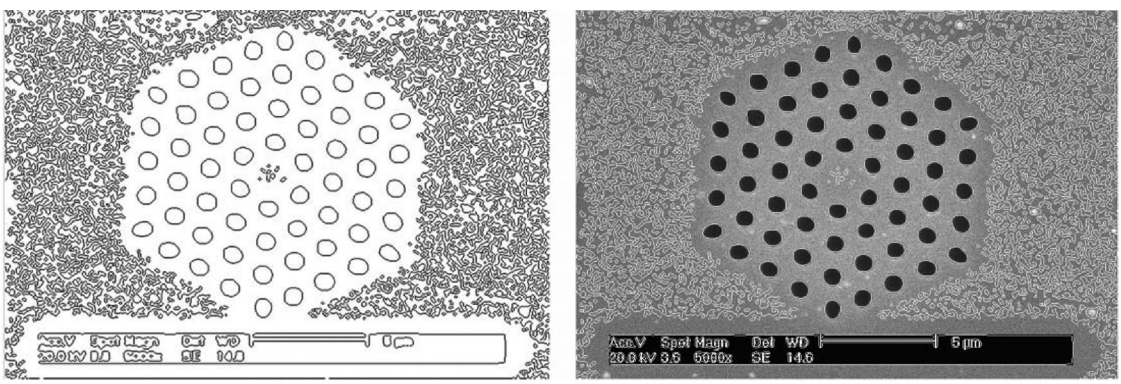

(a) (b)

DOI: 10.1109/JPHOT.2016.2614780
1943-0655 © 2016 IEEE

A Novel Method Based on Digital Image Processing Technique and Finite Element Method for Rapidly Modeling Optical Properties of Actual Microstructured Optical Fibers

Jianshe Li,[1] *Student Member, IEEE*, Shuguang Li,[1] Guanghua Gu,[2] Hui Li,[1] Qiang Liu,[1] Zhenkai Fan,[1] Hailiang Chen,[1] *Student Member, IEEE*, Xiaoming Han,[1] Yuanyuan Zhao,[1] and Pu Zhang[1]

[1]State Key Laboratory of Metastable Materials Science and Technology, College of Science, Yanshan University, Qinhuangdao 066004, China
[2]College of Information Science and Engineering, Yanshan University, Qinhuangdao 066004, China

DOI:10.1109/JPHOT.2016.2614780

Manuscript received June 16, 2016; revised September 24, 2016; accepted September 27, 2016. Date of publication October 10, 2016; date of current version October 24, 2016. This work was supported by the National Natural Science Foundation of China under Grant 61178026, Grant 61475134, Grant 61505175, and Grant 61303128; in part by the Natural Science Foundation of Hebei Province, China, under Grant E2012203035; and in part by the Doctoral Foundation of Yanshan University under Grant B1004. Corresponding author: S. Li (e-mail: shuguangli@ysu.edu.cn).

Abstract: The cross-section image of microstructure optical fiber (MOF) is usually characterized by the irregular shape, disordered distribution of the air pores, and multiple sources of noise. The traditional modeling of fiber structure does not work for these MOFs, and it is difficult to obtain the actual cross-section structure. A new method based on the digital image processing technique and finite element method (FEM) is introduced. With this method, the actual cross-section structure of MOFs can be rapidly modeled by gray scale processing, filtering, threshold, and edge detection, which is vital to the simulation of the basic properties of the fiber with FEM precisely. The method is proved to be feasible and reliable in that the dispersion coefficients of an actual fiber simulated are greatly consistent with the experimental results. In addition, the influence of perfect matched layer thinkness, as well as the curve fitting interval selection of the dispersion coefficients on the research results, is explored in the paper, which forms a basis for the correct setting of these parameters. The method has the advantages of strong adaptability, good modeling effect, rapid simulation, and accurate results. Finally, the method applies to all kinds of cross-section modeling of fiber, especially for disordered structure modeling.

Index Terms: Microstructured fibers, digital image processing, fiber optics imaging, nonlinear optics.

1. Introduction

Due to the flexibility of structure design and the sensitivity to structural change, MOF has been a popular topic focused on by researchers since it was original proposed [1], [2], and a new research in the fields of nonlinear and optical fiber optics has started. The flexibility of structure design of the

MOFs makes them have the characteristics of high tunable properties in many respects, such as guided mode [3], dispersion [4], [5], nonlinearity [6], [7], birefringence [8], polarization [9], and so on. In fact, the comprehensive characteristics of the MOFs are based on the difference of various factors. For instance, the different components of the optical fiber, the fiber core, the size, the shape, the position, and the arrangement of the air holes will directly affect the final quality of optical fiber and even play a decisive role.

Generally at the moment, in the MOFs′ research, researchers first design the fiber structure and optimize the fiber properties by using the finite element [10] or multipole methods [11], and then fabricate the fiber by stacking and extruding. In the process of drawing optical fibers, many irregular air holes will collapse and displace influenced by gravity, drawing temperature control, drawing speed and other factors, which will cause the structure of fabricated fibers not to conform to the theoretical design. This will seriously affect the performance of the fiber. Therefore, the change of the optical fiber characteristics caused by the deformation of structure cannot be ignored. In the past, in most references, researchers usually treat them as ideal hexagonal structure and have even idealized the cross-section of random distribution holes as standard graphics when modeling the cross-section of actual fiber with defect. Obviously, the more complex the cross-section image of PCFs, the greater the error will be.

Along with research, more scientific and more practical modeling methods have been proposed. Yao *et al.* proposed a numerical analysis method based on the combination of image processing algorithms and the finite difference frequency domain [12]. Based on numerical analysis methods of thresholding segmentation and Wiener filtering, the optical fiber section geometry image is obtained by using scanning electron microscopy image of photonic crystal fiber. The zero dispersion wavelength values which simulated by processing image modeling are a high coincidence with experimental values. S. Lou task group proposed two methods based on the digital signal processing technology [13], [14] and the point spread function of Kalman filter [15] combined with finite element method to accurately evaluate the real optical properties of the MOFs. In these methods, they mainly solve the defects of optical fiber end face image. Besides, some digital image processing skills of histogram and filter processing are also included. Hlubina *et al.* adopted the method of modifying the histogram to handle the cross-section image [16], [17]. Histogram modification is a common method of digital image processing, and although the authors did not detail the specific steps of solutions, the processing effects are ideal through the results. The Sobel operator is used in the MOF cross-section image processing in [13].

The publication of these documents has greatly enriched the ideas and methods of the cross-section processing. Considering that the actual processing cross-section is often characterized by a great deal of randomness, a novel method based on digital image processing technique and finite element method is proposed to simulate the MOF property with arbitrary structure in this paper and is verified by examples. The verification shows that the simulation and experiment are in good agreement, which proves the method to be correct and scientific. In this paper, based on the concept of combination parameter design, each set of different parameters can be sucessfully mapped to a different kind of practical optical fiber end face pattern. Therefore, the concept has the advantages of good processing effect, strong operability and high adaptability to the image source of the optical fiber end face, which are not available in other papers.

2. Digital Image Processing Technology in the Application of Cross-Section Processing

The presence of air holes results in the uneven intensities of the cross-section structure of MOF, which causes the fiber to break easily when it is cut with a cutting knife. When such a cross-section is observed with a microscope (such as scanning electron microscope (SEM),conventional microscope,optical microscope, and so on), the uneven cutting will generate fuzzy noise owning to different depth in the cross-section iamge (such as area 1 in Fig. 1). In addition, due to the small size of the fiber used for sampling, it it not easy to fasten the sampling optical fiber, or it may

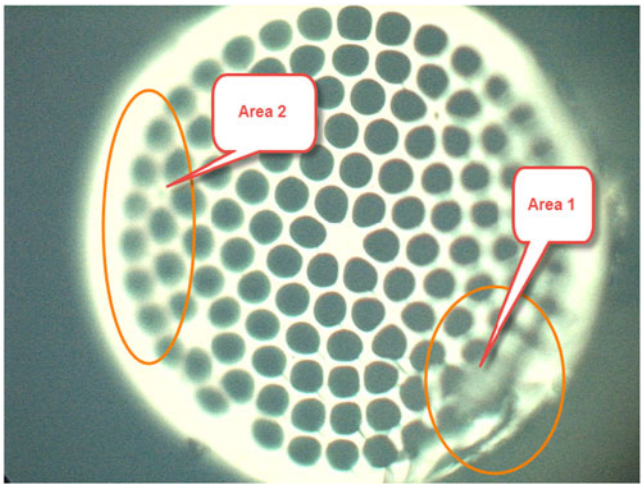

Fig. 1. Cross-section of PCF with obvious noise.

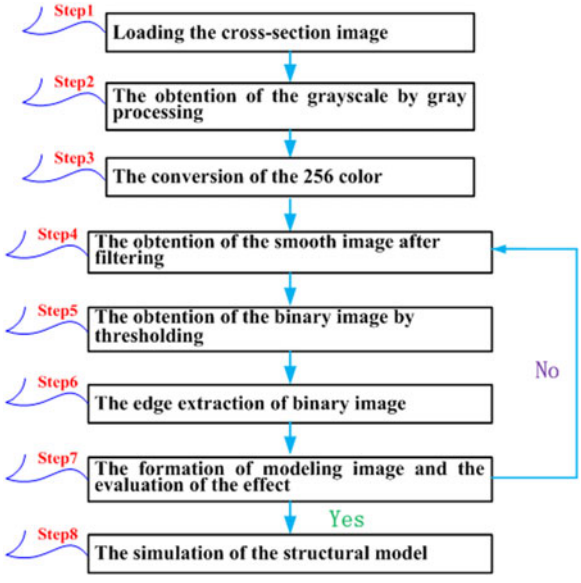

Fig. 2. Flow chart.

prodece depth fuzzy noise for the cross-section is not in parallel with the objective lens (such as area 2 in Fig. 1). Besides, the sensor noise, the optical system aberration, and the scattering of the light source are the reasons for the formation of imaging noise.

Given that the actual cross-sections of MOFs are complex, the noise sources are widely existed. In this paper, we proposed a set of solution based on digital iamge processing technilogy. It can be widely applied to the “weakening” treatment of the common noise in the MOF cross-section image and easy to derive the ideal treatment effect iamge, thus displaying a faithful structural modeling for the applicatio of FEM. The program flow chart is shown in Fig. 2.

2.1 Gray Processing and 256 Color Conversion (Corresponding to Step 1–Step 3, as Shown in Fig. 2)

The cross-section image obtained by the microscope is generally RGB image, which is developed by the mixing principle of the three primary colors of light in nature. RGB represents red, green, and

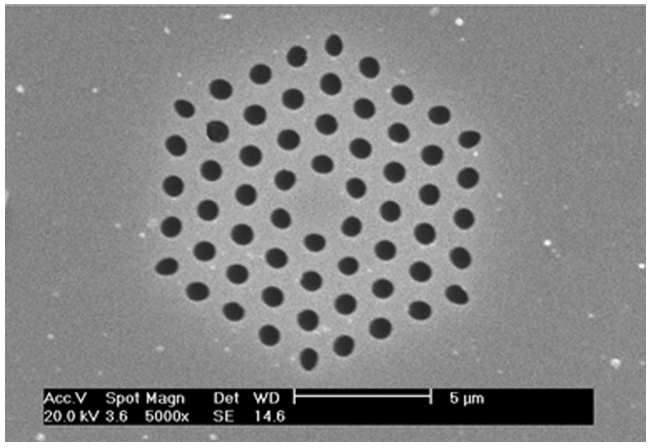

Fig. 3. Cross-section image of MOF obtained by SEM.

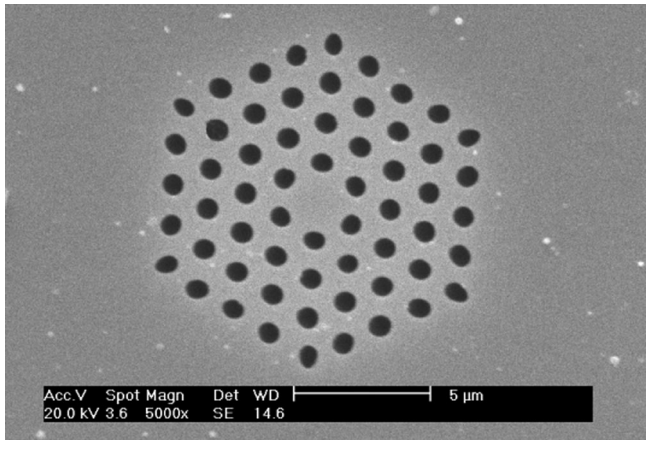

Fig. 4. Grayscale image after processing.

blue, respectively. Each pixel in each color can load the eighth power of 2 (in total 256) brightness levels. The three color channels are combined together to reflect the cube of the 256 (about 16 700 000) color changes. We are mainly interested in the fringe areas of holes instead of the color information of the image, when the cross-section image is dealt with. Therefore, in order to facilitate the processing, it needs to transform the RGB image into the gray scale image first, and limit the range to [0, 255]. Gray scale image is stored in the form of one dimensional matrix, and the value of each point within the matrix represents the image brightness at the point. Fig. 3 is the cross-section image of the optical fiber obtained by SEM. Fig. 4 is the gray scale image after processing. Since the Fig. 3 in this paper is yet the gray scale image, the difference between Figs. 4 and 3 is not great. But as a general rule, the original image can be RGB image.

2.2 Filtering of Butterworth High-Pass filter (Corresponding to Step 4, as Shown in Fig. 2)

Analyzing the image features of Fig. 1, we can see that the locations of the holes are darker than the other regions, because the reflectance imaging is usually used for the cross-section image. As we know, the edges and the abrupt change parts of the image are related to the high frequency components, while other large areas are mainly composed of low frequency components. Therefore,

the frequency domain processing method can effectively limit the low frequency components and emphasize the high-frequency component of the image edge, which lays a foundation for the edge extraction.

The Butterworth filter is commonly used in the digital image processing. The curve of frequency response in the pass-band keeps maximally flat, while the stop-band is decreased to zero. The relatively gentle changes in pass-band can effectively reduce the vibration generated in the process of filtering and prevent the formation of white noise inside the holes or black noise in the background areas after filtering. Our research shows that Butterworth high pass filter [18] is an ideal method for image filtering. By convolution theorem

$$G(u, v) = H(u, v) \cdot F(u, v) \tag{1}$$

where $F(u, v)$ is the Fourier transform consisting of images containing noise. $G(u, v)$ is the Fourier transform of the image after filtering. $H(u, v)$ is the transfer function. The key to filtering is to select the appropriate $H(u, v)$. By using the transfer function, for $F(u, v)$ the low frequency components are attenuated and the high frequency components can be preserved. The smooth image $g(u, v)$ can be obtained through a Fourier transform after the $G(u, v)$ obtained. The transfer function of the Butterworth high pass filter can be expressed by the following formula:

$$H(u, v) = \frac{1}{1 + m\left[\frac{D_0}{D(u,v)}\right]^{2n}} \tag{2}$$

where $D(u, v) = [u^2 + v^2]^{0.5}$ represents the distance from the origin to the (u, v) point in the frequency domain. D_0 is the cutoff frequency. m is the transformation coefficient, which is usually 0.414. n is the filter order. In terms of u and v, $H(u, v)$ is a three-dimensional graphics, and its section plan, stereogram and planform are shown in Fig. 5. Fig. 5(a) is a variation between $H(u, v)$ and $\frac{D(u,v)}{D_0}$ when n is 2. Rotating it by 360° around the axis, we can obtain Fig. 5(b). Fig. 5(c) can be obtained from a projection on the $u - v$ plane of Fig. 5(b). In the transfer function, the transfer function curve is different which depends on the cutoff wavelength D_0 and the order number n. These flexible parameter settings will greatly improve the adaptability of the sampling cross-section. All the frequency components in the sample image are filtered by the transfer function depicted in Fig. 5. Fig. 5(a) shows that the lower the frequency is, the greater and faster the signal attenuation is; while the higher the frequency is, the smaller and the slower the attenuation is, and more smooth the curve is. Therefore, the Butterworth high pass filter can quickly attenuate the frequency components within $\frac{D(u,v)}{D_0} < 1$, preserving the high frequency section, in which the highest frequency components can pass the filter nearly with no any damage. The low frequency parts represented by background are weakened and the high frequency components represented by the air holes are extruded. These make the boundary of air holes more acute. Fig. 6 is obtained after filtering.

2.3 Binary Image Is Obtained by Thresholding Smooth Image After Filtering (Corresponding to Step 5 as Shown in Fig. 2)

The matrix $J1(I, J)$ is the stored matrix for the data of the smooth image after filtering. For each element of the $J1(I, J)$ matrix, the threshold segmentation is done. The set threshold is q. A black and white binary image is obtained by setting all the elements greater or equal to q in the matrix as 225, while it is less than q as 0. Normally, the value of q ranges as the following rules: (1) If background color of the image is very close to the holes, the range of q is $0 < q \leq 125$. (2) If they are really different, the range of q is $125 < q \leq 255$, but this is not categorical. The optimal evaluation of q is also determined by other parameters, such as the cut-off frequency. In practice, q can be carried out in a large range which is greater than 0, and less than or equal to 255 to tune up the effect. The method has the great flexibility in the processing of cross-section image, and also ensures the high adaptability to process the wide noise source. Fig. 7 is the binary image after the threshold. In Fig. 7, q is 5.

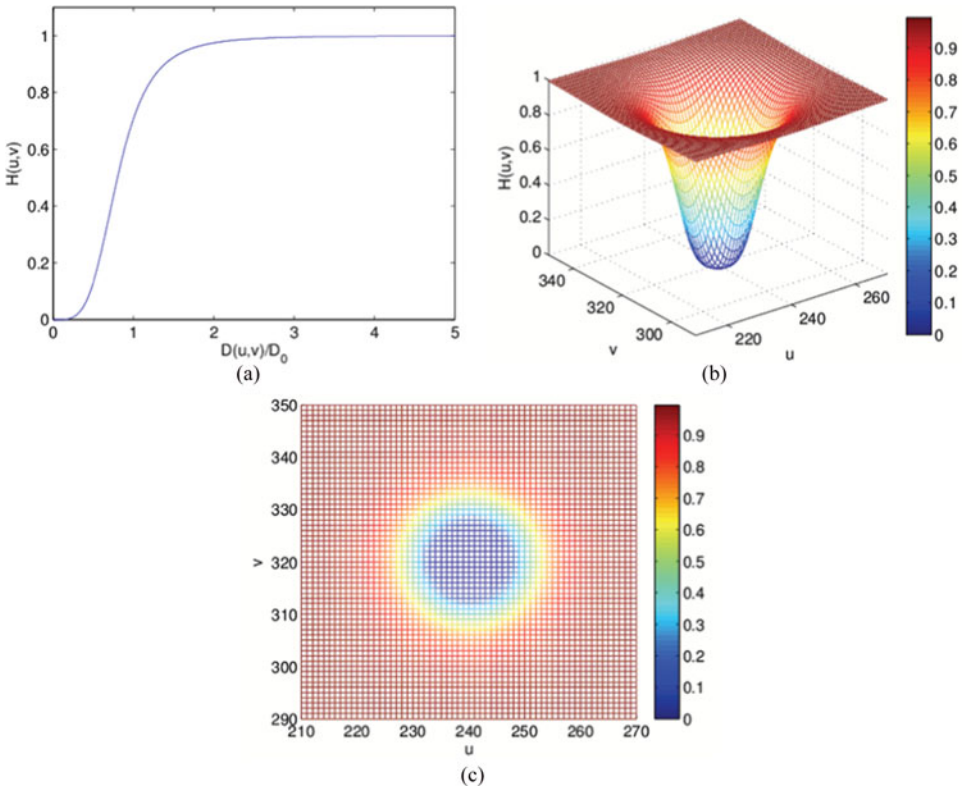

Fig. 5. Transfer function diagram of Butterworth high pass filter. (a) Section plan ($n = 2$, $m = 0.414$). (b) Stereogram. (c) Planform.

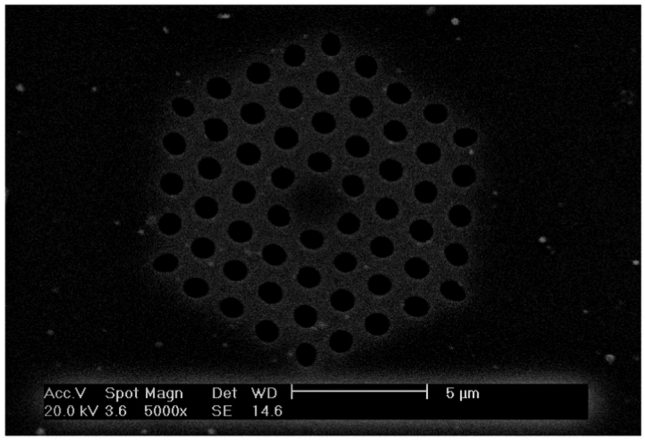

Fig. 6. Image obtained after filtering.

2.4 Edge Extraction and Geometry Formation and Effect Evaluation (Corresponding to Step 6 ~ Step 7, as Shown in Fig. 2)

Using the edge extraction algorithm Canny operator [19], fiber modeling image is obtained by extracting the edge of Fig. 7. Canny operator is a class of optimal edge detection operator. It detects strong edges and weak edges, respectively, by using two different thresholds. The weak edges are included in the output image, when the weak edges are connected to the strong edges.

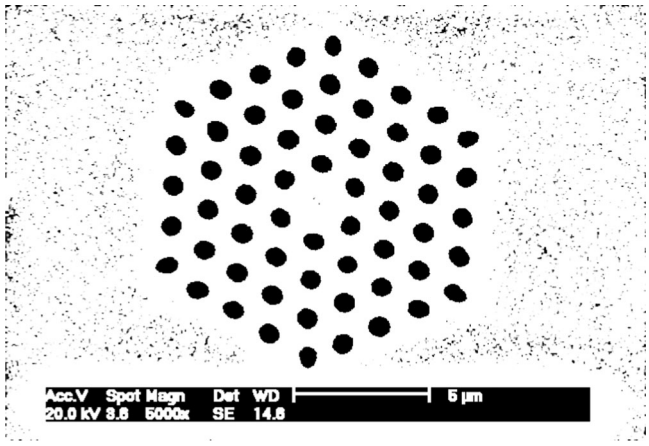

Fig. 7. Binary image obtained by thresholding.

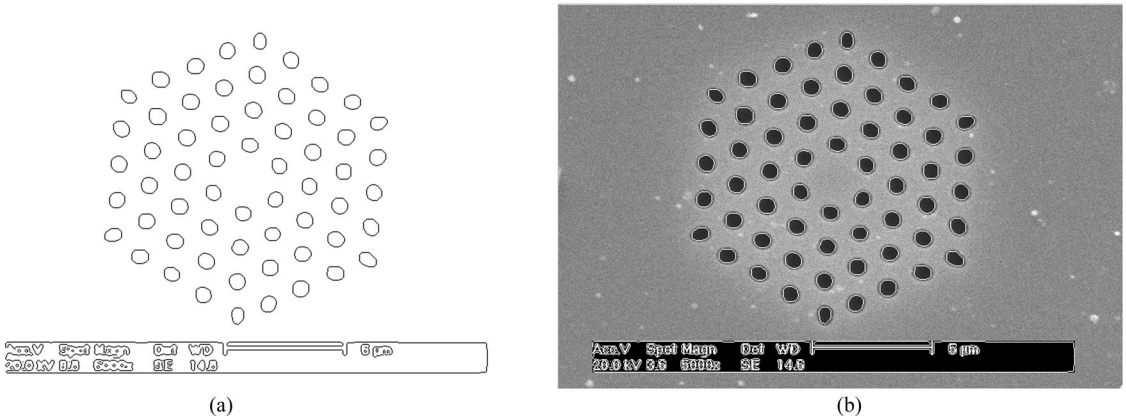

(a) (b)

Fig. 8. (a) Processing effect when parameters D_0, n, m, and q are 14, 2, 0.414, and 5, respectively. (b) Effect exhibition after the superposition of the extraction of the edge of holes and chosen parameters are as (a) and Fig. 3.

The advantage of the Canny operator is that all the edges can be identified with no any missed detection or wrong detection, thus ensuring the accuracy of the edge extraction.

In actual processing, different edge extraction images can be obtained by different combination parameters, which include the cutoff frequency, the order of filter, the coefficient m and the threshold q shown in Figs. 8–10. The values of the parameters D_0, n, m and q are 14, 2, 0.414 and 5 respectively in Fig. 8. In Fig. 9, the values of the parameters D_0, n, and m are 14, 2, 0.414 respectively, and in the threshold processing, all the nonzero elements of the matrix $J1$ are forced to be converted to 255. The values of the parameters D_0, n, m and q are 8, 2, 0.5, and 5 respectively in Fig. 10. Comparing the processing image with the actual cross-section of MOF, the combination parameters are reserved and the next step is beginning, as the processing effect is ideal. The combination parameters are optimized until it is ideal, as the effect is not good.

The evaluation of image processing effect can refer to the folowing standards: 1) The parameters are selected when the processing effect of most the air holes is ideal. 2) The edge profile of air holes consists of smooth and continuous curve rather than broken lines. 3) In the superposed graph, the size of the extracted holes can not be obviously greater or less than the size of corresponding holes in the original graph. 4) The processing effect of the air holes near the fiber core are preferentially considered, as these holes have greater influence on fiber properties. 5) If the processing effect of

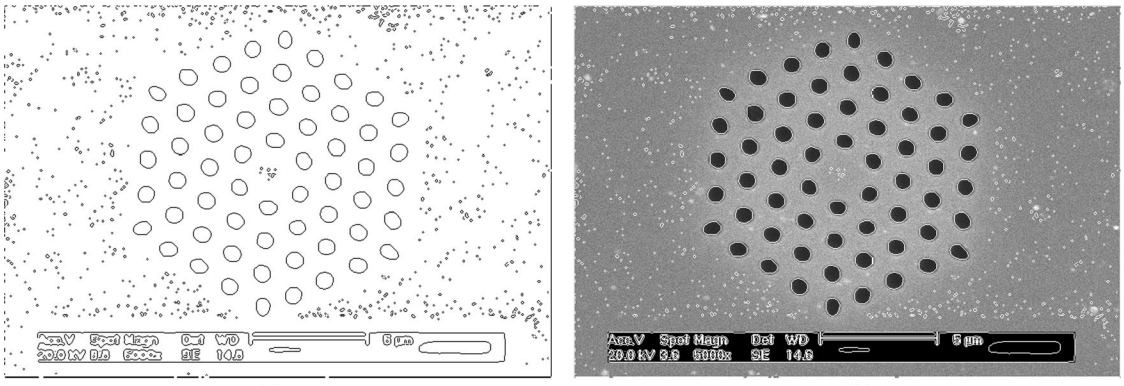

(a) (b)

Fig. 9. (a) Processing effect when parameters D_0, n, and m are 14, 2, and 0.414, respectively, and all the nonzero elements of the matrix $J1$ are forced to be converted to 255. (b) Effect exhibition after the superposition of the extraction of the edge of holes, and parameters are as (a) and Fig. 3.

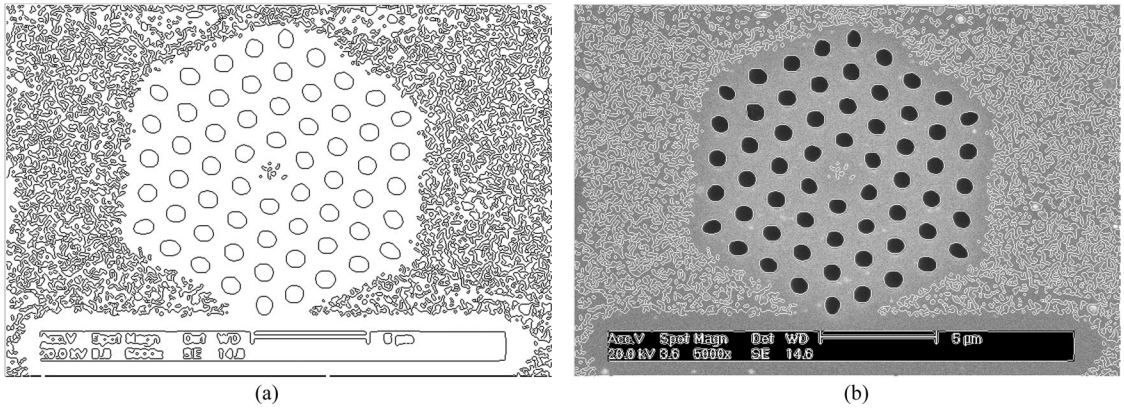

(a) (b)

Fig. 10. (a) Processing effect when parameters D_0, n, m, and q are 2, 2, 0.5, and 5, respectively. (b) Effect exhibition after the superposition of the extraction of the edge of holes, and parameters are as (a) and Fig. 3.

most airholes are very good, while the edge extraction of individual air holes are incomplete due to the quality of original graph, and these air holes can be revised according to original graph by two order Bessel curve in Comsol. By comparing Figs. 8(b)–10(b), we can see that the edge extraction and original image are in best agreement with those in Fig. 10. Obviously, the size of air holes in Fig. 8 is less than the original graph, while the number of broken line in the holes edge is more than Fig. 10. So in the following simulation, we choose the parameters of Fig. 10(a) for the model.

2.5 Finite Element Simulation for Structural Modeling (Corresponding to Step 8, as Shown in Fig. 2)

By importing the edge detection image into the finite element software Comsol to simulate, we can obtain the refractive index relationship at different wavelengths, which is the basis property to simulate the fiber. It is notable that the conversion of graphic unit and coordinate proportion must be carried out when the picture is imported, as the default unit of Comsol is the international unit m. The specific method is as follows: First, the image scale of picture is imported along with the image, then the length x_1 of the scale line is read in Comsol (unit m). If the scale line of the original image represents the value of x_0 (unit m), in Comsol, the zoom factor x can be obtained by $\frac{1(\mathrm{m})}{x_1(\mathrm{m})} = \frac{x}{x_0(\mu\mathrm{m})}$, and the x's unit is μm. Second, the image scale of picture and the excess portion of the modeling image after processed in the Comsol are removed, and then, the model can be

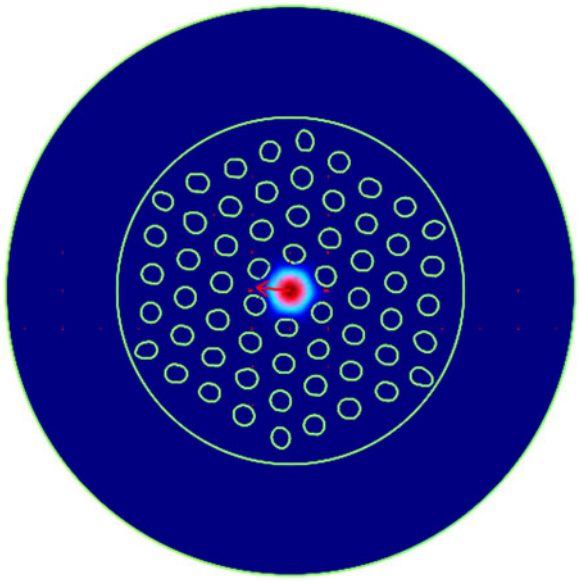

Fig. 11. Optical fiber model and the fundamental mode field.

done by using the coefficient x_2 (x_2 is equal to x numerical and has no dimension) to zoom the whole image. Finally, the model is solved by the finite element method [20], and the relationship between the effective refractive index and wavelength can be obtained. Fig. 11 shows the model of the optical fiber and the simulation of this model. In this case, $x_1 = 1.51$ m, $x_0 = 5$ μm, the zoom factor is $x_2 = 3.31125828 \times 10^{-6}$. Specially, the order of minimum unit in Comsol drawing module is about 10^{-14} m. In order to improve the modeling accuracy, we set the order of zoom factor as 10^{-14} or 10^{-15}. The outer radius of PML is set as $x_{or1} = 11$ μm, and the inner radius is set as $x_{ir1} = 6.7$ μm.

3. Simulation of the Fiber's Basic Parameters and the Test of the Correctness of its Processing Method

A_{eff} is the effective mode area of the optical field. It can be defined as

$$A_{eff} = \frac{\left[\int_{-\infty}^{+\infty}\int_{-\infty}^{+\infty} |E(x,y)|^2 dxdy\right]^2}{\int_{-\infty}^{+\infty}\int_{-\infty}^{+\infty} |E(x,y)|^4 dxdy} \tag{3}$$

where E(x,y) is the transverse electrical field component of the fundamental fiber mode. First, we get the fundamental fiber mode at a operating wavelength with Comsol. Second, we select "Electric field,norm" in subdomain integration under postprocessing and set the electric subdomain. At last, the operation of electric field norm as (3) can be finised by writing program code in Matlab keeping synchronous communication connection with Comsol, and the effective mode area at a operating wavelength can be obtained. The effective mode area at different operating wavelength can be obtained by wavelength scanning. A_{eff} is the visual reflection of the strength of restricted right, whose value has a great relationship with the structural parameters of MOF.

The nonlinear coefficient γ of optical fiber is defined as [21]

$$\gamma = \frac{2\pi n_2}{\lambda \cdot A_{eff}} \tag{4}$$

where n_2 is the nonlinear refractive index coefficient of materials. λ is the operating wavelength. A_{eff} is the effective mode area of optical field. The key to solve the nonlinear coefficient is reasonable

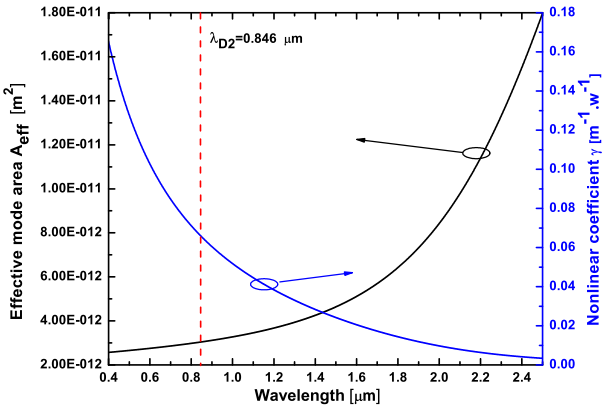

Fig. 12. Effective mode area and the nonlinear coefficient of the fundamental mode relying on wavelength by simulation.

setting of the electric subdomain, because n_2 of the base materials and the air in the holes are different. During our simulation, for the silica, it is 2.7 $\times 10^{-20}$ m^2/W [22], and for air, it is 2.9 $\times 10^{-23}$ m^2/W. The value of nonlinear coefficient γ is directly related to the strength of the nonlinear of MOF, which is a important index to measure the quality of MOF. When the material and the operating wavelength are determined, the nonlinear coefficient γ is depend on A_{eff}. The smaller the A_{eff}, the greater the γ. The dispersion parameter D is defined as [21]

$$D = -\frac{\lambda}{c}\frac{d^2\mathrm{Re}(n_{eff})}{d\lambda^2} \tag{5}$$

where c is the propagation velocity of light in vacuum. λ is the operating wavelength. n_{eff} is the effective refractive index of the fundamental mode by simulating with the finite element method. In the calculations the material dispersion of silica is considered by the Sellmeier equation [23]

$$n(\lambda) = \sqrt{1 + \sum_{j=1}^{m} \frac{B_j \lambda^2}{\lambda^2 - \lambda_j^2}} \tag{6}$$

where $B_1 = 0.6961663$, $B_2 = 0.4079426$, $B_3 = 0.8974794$, $\lambda_1 = 0.0684043$ μm, $\lambda_2 = 0.1162414$ μm, and $\lambda_3 = 9.896161$ μm. The unit of λ is μm. As we all know, The dispersion parameter is an important index to measure the performance of the fiber dispersion. At the same time, it also determines the normal and anomalous dispersion region of the fiber. It also has influence on the nonlinear effect. From (5), we can see that the key to solve the dispersion parameter is the correct solution of the effective refractive index of the fiber mode, which depends on the fiber structure.

In conclusion, the most important thing to obtain the essential attribute(consisting of the effective mode area, the nonlinear coefficient and the dispersion parameter) of the fiber is to reconstruct the cross-section of the fiber. Using the method mentioned, we can accurately extract the real cross-section of the fiber. At this time, simulation to obtain the essential attribute of fiber becomes simple, rapid and accurate. we simulate the effective mode area of the the fundamental fiber mode A_{eff} and the nonlinear coefficient γ relying on wavelength in Fig. 12. Fig. 13 shows the dispersion parameter D of the fundamental mode relying on wavelength.

4. Discussion

4.1 Calculation of the Mode Effective Refractive Index Relying on the Setting of the Thickness of PML

In the above steps, the outer radius of PML is $r_{or1} = 11$ μm, while the inner radius is $r_{ir1} = 6.7$ μm. The thickness is $T_1 = r_{or1} - r_{ir1} = 4.4$ μm. With these parameters, the real part of the mode

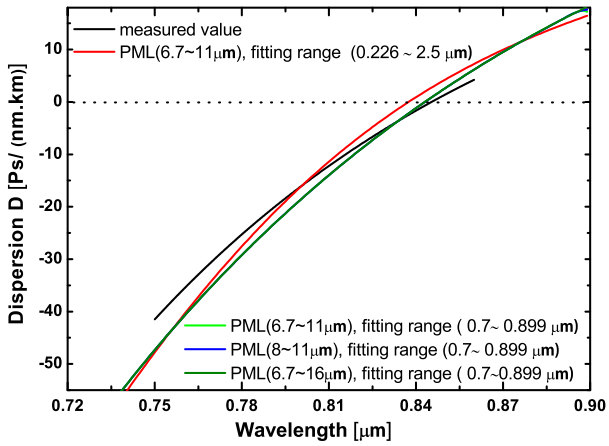

Fig. 13. Dispersion parameter of the fundamental mode relying on wavelength. The black curve line is the value by experimental measurement, while the other curve lines is the value by simulation. In the simulation, the thickness of the PML is about 6.7 $\sim$ 11 μm, and the fitting range is 0.226 $\sim$ 2.5 μm in the red curve line. For the green curve line, the two parameters are, respectively, 6.7$\sim$ 11 μm and 0.7 $\sim$ 0.899 μm. For the blue curve line, they are, respectively, 8 $\sim$ 11 μm and 0.7 $\sim$ 0.899 μm. For the olive green curve line, they are, respectively, 6.7 $\sim$ 11 μm and 0.7 $\sim$ 0.899 μm.

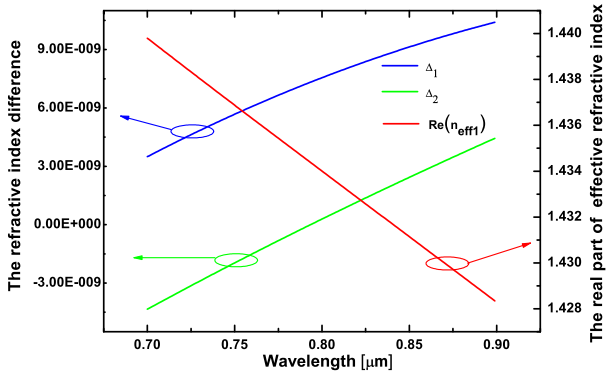

Fig. 14. Real parts of the mode effective refractive indexes (red curve line) and the differences betweem them (blue and green curve lines) relying on the wavelength with three different thicknesses of PML.

effective refractive index relying on the wavelength is shown as the red curve line in Fig. 14. To discuss the influence by the thickness of PML on the real part of effective refractive index, we set other two sets of parameters to show the influence. Two sets of parameters are $r_{ir2} = 8$ μm, $r_{or2} =$ 11 μm, $T_2 = 3$ μm and $r_{ir3} = 6.7$ μm, $r_{or3} = 16$ μm, $T_3 = 9.3$ μm, respectively. To see the difference, we set $\Delta_1 = \mathrm{Re}(n_{eff2}) - \mathrm{Re}(n_{eff1})$ and $\Delta_2 = \mathrm{Re}(n_{eff3}) - \mathrm{Re}(n_{eff1})$ as vertical coordinates and obtain the blue and green curve lines in Fig. 14. The differences betweem effective refractive index are quite small for the three sets of parameters as shown in Fig. 14, the orders of the Δ_1 and Δ_2 are about 10^{-9}. It is illustrated that the setting of the thickness of PML has only a small effect on the calculation of the mode effective refractive index. This is because that PML is artificial boundary to obtain the numerical solution of the characteristic equation. During the simulation, it is suitable when the unit of the thickness is equal to or a little larger than the unit of wavelength.

4.2 Influence by the Interval Selction When the Dispersion Coefficient is Fitted on the Calculation of Dispersion Parameter D

From (5), we need to solve the second derivative of $\mathrm{Re}(n_{eff})$, before the calculation of D. As $\mathrm{Re}(n_{eff})$ and λ are discrete numerical correspondence, the fitting for them during the calculation

is demanded. During the fitting, the interval selction of independent variable λ has effect on the calculation of D. To reflect it, we compare with two groups parameters and show them in Fig. 13. When the thickness of the PML is T_1 and the fitting range is 0.226 $\sim$ 2.5 μm, D relying on λ is shown as the red curve line in Fig. 13, the zero dispersion wavelength is $\lambda_{zero1} = 0.838$ μm. the thickness of the PML is still T_1 and the fitting range is 0.7 $\sim$ 0.899 μm, D relying on λ is shown as the green curve line in Fig. 13, the zero dispersion wavelength is $\lambda_{zero2} = 0.843$ μm. When the two parameters are respectively T_2 and 0.7 $\sim$ 0.899 μm, D as a function of λ is shown as the blue curve line in Fig. 13, the zero dispersion wavelength is also $\lambda_{zero2} = 0.843$ μm. We can see that the blue curve line and the green curve line coincide absolutely. When the two parameters are respectively T_3 and 0.7 $\sim$ 0.899 μm, D as a function of λ is shown as the olive green curve line in Fig. 13, the zero dispersion wavelength is also $\lambda_{zero2} = 0.843$ μm. Similary, the olive green curve line coincide with the blue and green curve lines.

The contrast between the red curve line and the green curve line illustrates that the fitting results are different even with the same discrete value of Re(n_{eff})-λ. In addition, the fitting results are identical even with the different thickness of PML. It follows that the interval selction has greater influence than the thickness of PML on the simulation results when the dispersion coefficient is fitted. In Fig. 13, there are two points of intersection between the red curve line and the green curve line, while the bending of the red curve line is bigger. It is illustrated that the bigger the interval selction, the bigger the bending of fitting curve. Therefore, the interval selction is much more important. In the simulation of the fiber properties, ideal results can be obtained by selecting calculated interval rather than a bigger interval.

The black curve line is obtained by experimental measurements [12] with white light interferometry (low coherence interferometry) [24], [25]. The zero dispersion wavelength is also $\lambda_{zero0} = 0.845$ μm. The white light interferometry is one of the most effective methods to measure the Chromatic Dispersion of short fiber in the experiment. The Dispersion function is obtained by fitting the interference spectrum using nonlinear curve fitting method during the postprocessing. Its processing accuracy is realy high, whose resolution is as high as 0.1/ps [25].

The curves in Fig. 13 have high degree of agreement within the scope of drawing. The deviation between λ_{zero1} and λ_{mzero} is $\varepsilon_1 = |\lambda_{zero1} - \lambda_{mzero}|/\lambda_{mzero} = 0.83\%$, while the deviation between λ_{zero2} and λ_{mzero} is $\varepsilon_2 = |\lambda_{zero2} - \lambda_{mzero}|/\lambda_{mzero} = 0.24\%$. For parameter D, the small deviation between the simulation and the experiment sufficiently illustrate the accuracy and the correctness.

We discuss the influence of the number of data points in the fitting interval to the fitting results. In Fig. 13, black curve has a total of 1001 discrete data points at the range of 0.75 $\sim$ 0.86 μm, while green curve, blue curve and olive green curve have 200 discrete data points at the range of 0.7 $\sim$ 0.899 μm respectively. In particular, the fiber structure model corresponding to the red curve and green curve are exactly the same. However, the red curve fitting interval in solving the dispersion coefficient interal is selected the range of 0.226 $\sim$ 2.5 μm and has 2275 discrete data points at this range, the green curve is 0.7 $\sim$ 0.899 μm and the red curve has 200 discrete data points at this range. The original datas of these curves for fitting are derived from simulation of the refractive index of the base model by the finite element method. The wavelength interval is selected 1 nm which is close to the minimum wavelength of the finite element method to accurate simulations. By comparing the red curve with the green one, we can see that even though the fitting sample date are completely consistent. If the selection of the fitting interal is inconsistent, it will lead to inconformity of the fitting curve and the radius of curvature of the fitting curve increases as the data points in fitting ranges increase. By comparing red curve, green curve, blue curve, and olive green curve, we proposed that as a result there is no necessary connection between the number of data points and the fitting results, and the fitting results are mainly determined by the choice of fitting interval.

4.3 The Processing the Ordinary Optical Microscope Images

Not only can it deal with the scanning electron microscope images, but it can also deal with the ordinary optical microscope images. Fig. 15(b) shows the processing of the ordinary optical

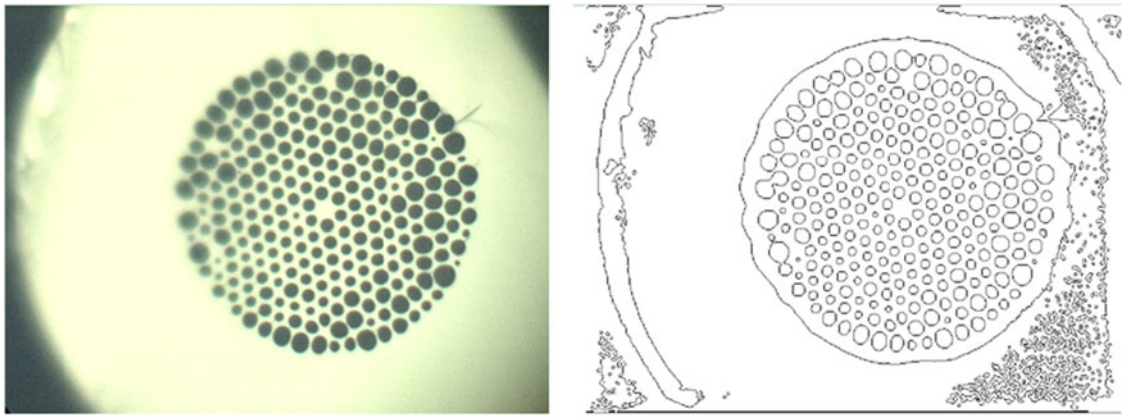

Fig. 15. Processing of the ordinary optical microscope images. (a) Original image. (b) Image of the fiber structure with the initial image processing.

microscope images. From this, we can see that the fiber structure is extracted and the holes near the fiber core are accurately extracted, while the outer holes can be modified by two order Bezier curve in COMSOL. According to the principle of guiding light for MOF, the error caused by the modification can be ignored.

5. Conclusion

This paper presents a novel method based on digital image processing technique and finite element method, which can be widely used to deal with or "weaken" the fuzzy and motion noise in the cross-section image. The method has the merits of strong adaptability, good modeling effect, rapid simulation and accurate result. By comparison, we find that the dispersion coefficients by theoretical simulation and actual measurement are in good agreement, which demonstrates the correctness and the scientificity of the method. This method is also adopt successfully to our former work [26]. The influences on the calculation are analyzed. We found that the thickness of PML has no different for the calculation of the mode effective refractive index in a reasonable range. In addition, the interval selction have a great effect on the simulation when the dispersion coefficient is fitted. Therefore, it is important to select calculated interval when the dispersion coefficient is fitted.

The method has wide applicable range. Not only can it deal with only the SEM images, but it can also deal with the ordinary optical microscope images. This method only needs a cross-section image to simulate the properties of the optical fiber. The reconstruction code of the cross-section model is run on the personal computer, and the operation time is generally controlled within 2 seconds, which is a great progress of technology.

The progress of the cross-section image processing can further weaken the influence by the inaccuracy of the cross-section image and can further compress the noise source which cause uncertain disturbances. It is realy an positive influence to the research of MOF. Therefore, the method can be used for fast simulation of optical properties, as well as for real-time monitoring and rapid assessment during the drawing process.

Acknowledgment

The authors would like to thank Prof. Y. Li from the School of Precision Instrument and Opto-Electronics Engineering, Tianjin University, Tianjin, China, for providing the test image of the MOF cross-section and the experimental data of dispersion. The authors would like to thank the anonymous reviewers for their valuable comments that have improved the work presented in this paper.

References

[1] J. C. Knight, T. A. Birks, P. S. J. Russell, and D. Atkin, "All-silica single-mode optical fiber with photonic crystal cladding," *Opt. Lett.*, vol. 21, no. 19, pp. 1547–1549, Oct. 1996.

[2] T. A. Birks, J. C. Knight, and P. St. J. Russell, "Endlessly single-mode photonic crystal fiber," *Opt. Lett.*, vol. 22, no. 13, pp. 961–963, Jul. 1997.

[3] J. Fini, "Design of solid and microstructure fibers for suppression of higher-order modes," *Opt. Exp.*, vol. 13, no. 9, pp. 3477–3490, May 2005.

[4] S. Wabnitz, "Broadband parametric amplification in photonic crystal fibers with two zero-dispersion wavelengths," *J. Lightw. Technol.*, vol. 24, no. 4, Apr. 2006, Art. no. 1732.

[5] S. Yang *et al.*, "Theoretical study and experimental fabrication of high negative dispersion photonic crystal fiber with large area mode field," *Opt. Exp.*, vol. 13, no. 9, pp. 3015–3023, Apr. 2006.

[6] M. Liao *et al.*, "Fabrication and characterization of a chalcogenide-tellurite composite microstructure fiber with high nonlinearity," *Opt. Exp.*, vol. 17, no. 24, pp. 21608–21614, Nov. 2009.

[7] W. Su, S. Lou, H. Zou, and B. Han, "A highly nonlinear photonic quasi-crystal fiber with low confinement loss and flattened dispersion," *Opt. Fiber Technol.*, vol. 20, no. 5, pp. 473–477, Jul. 2014.

[8] T. Cheng *et al.*, "Fabrication and characterization of a hybrid four-hole $AsSe_2 - As_2S_5$ microstructured optical fiber with a large refractive index difference," *Opt. Exp.*, vol. 22, no. 11, pp. 13322–13329, May 2014.

[9] L. Zhang, S.-G. Li, Y.-Y. Yao, B. Fu, and M.-Y. Zhang, "Properties of high birefringence chalcogenide glass holey fibre for mid-infrared transparency," *J. Opt.*, vol. 12, no. 3, Feb. 2010, Art. no. 035207.

[10] F. Brechet, J. Marcou, D. Pagnoux, and P. Roy, "Complete analysis of the characteristics of propagation into photonic crystal fibers, by the finite element method," *Opt. Fiber. Technol.*, vol. 6, no. 2, pp. 181–191, Apr. 2000.

[11] T. White *et al.*, "Multipole method for microstructured optical fibers. i. formulation," *J. Opt. Soc. Amer. B*, vol. 9, no. 10, pp. 2322–2330, Oct. 2002.

[12] Y. Yao *et al.*, "Analysis of real photonic crystal fibers by finite-difference frequency domain method combined with digital image processing," *(in Chinese), Acta Optica Sinica*, vol. 28, no. 7, pp. 1384–1389, Jul. 2008.

[13] Y. Shen, L. Wang, and S. Lou, "Improved method for fast evaluating optical properties of actual photonic crystal fibers," (in Chinese), *Infrared Laser Eng.*, vol. 41, no. 4, Apr. 2012, Art. no. 037.

[14] L. Wang, S. Lou, W. Chen, and H. Li, "A novel method of rapidly modeling optical properties of actual photonic crystal fibres," *Chinese Phys. B*, vol. 19, no. 8, Aug. 2010, Art. no. 084209.

[15] Y. Shen, S. Lou, and X. Wang, "Estimation method of point spread function based on Kalman filter for accurately evaluating real optical properties of photonic crystal fibers," *Appl. Opt.*, vol. 53, no. 9, pp. 1838–1845, Mar. 2014.

[16] P. Hlubina *et al.*, "Measurement and modelling of dispersion characteristics of a two-mode birefringent holey fibre," *Meas. Sci. Technol.*, vol. 17, no. 4, Feb. 2006, Art. no. 626.

[17] P. Hlubina, M. Szpulak, D. Ciprian, T. Martynkien, and W. Urbanczyk, "Measurement of the group dispersion of the fundamental mode of holey fiber by white-light spectral interferometry," *Opt. Exp.*, vol. 15, no. 18, pp. 11073–11081, Sep. 2007.

[18] S. Butterworth, "On the theory of filter amplifiers," *Wireless Engineer*, pp. 536–541, Oct. 1930.

[19] J. Canny, "A computational approach to edge detection," *IEEE Trans. Pattern Anal. Mach. Intell.*, vol. PAMI-8, no. 6, pp. 679–698, Nov. 1986.

[20] S. Guenneau, A. Nicolet, F. Zolla, and S. Lasquellec, "Modeling of photonic crystal optical fibers with finite elements," *IEEE. Trans. Magn.*, vol. 38, no. 2, pp. 1261–1264, Mar. 2002.

[21] G. P. Agrawal, *Nonlinear Fiber Optics, 4th ed.* San Diego, CA, USA: Academic, 2006.

[22] E. Vogel, M. Weber, and D. Krol, "Nonlinear optical phenomena in glass," *Phys. Chem. Glasses*, vol. 32, no. 6, pp. 231–254, 1991.

[23] I. Malitson, "Interspecimen comparison of the refractive index of fused silica," *J. Opt. Soc. Amer.*, vol. 55, no. 10, pp. 1205–1208, Oct. 1965.

[24] S. Diddams, "Dispersion measurements with white-light interferometry," *J. Opt. Soc. Amer. B*, vol. 13, no. 6, pp. 1120–1129, Jun. 1996.

[25] P. Merritt and R. P. Tatam, "Interferometric chromatic dispersion measurements on short lengths of momomode optical fiber," *J. Lightw. Technol.*, vol. 7, no. 4, pp. 703–716, Apr. 1989.

[26] J. Li *et al.*, "Soliton and four-wave mixing effects induced by the third-order dispersion in a photonic crystal fiber with femtosecond pulses pumping at normal dispersion regime," *IEEE Photon. J.*, vol. 7, no. 5, Oct. 2015, Art. no. 3200211.